Research Article | Vol. 28, No. 24 / 23 November 2020 / Optics Express 36413
Optics EXPRESS

# Equivalent thin-plate method for stressed mirror polishing of an off-axis aspheric silicon carbide lightweight mirror

LIQI YI,[1,2] XUEJUN ZHANG,[1,*] HAIFEI HU,[1,3] ZHIYU ZHANG,[1] XUEFENG ZENG,[1] XIAO LUO,[1] DONGLIN XUE,[1] AND GE ZHANG[1]

[1] *Key Laboratory of Optical System Advanced Manufacturing Technology, Changchun Institute of Optics, Fine Mechanics and Physics, Chinese Academy of Sciences, Changchun, Jilin 130033, China*
[2] *University of Chinese Academy of Sciences, Beijing 100049, China*
[3] *School of Mechanical and Aerospace Engineering, Jilin University, Changchun, Jilin 130022, China*
[*] *zxj@ciomp.ac.cn*

**Abstract:** No physical model of stressed mirror polishing, based on the small deflection and deformation of elastic thin plates, has been applied in processing lightweight mirrors. We propose an equivalent thin-plate method for the stressed loading of lightweight mirrors for the first time. Stressed loading and polishing of an aspheric lightweight mirror are simulated using the small-deflection deformation theory of an elastic thin plate. We simulate off-axis aspheric silicon carbide (SiC) lightweight mirrors with three different structures, determining the corresponding equivalent thickness plate in a lightweight structure with a nearly uniform surface density distribution and isotropic bending properties. We then establish a residual removal model of a stressed polishing surface, design the stressed loading equipment, and propose an iterative method for stressed polishing of an off-axis aspheric SiC lightweight mirror. The results demonstrate that it is feasible to choose a lightweight structure that performs full-aperture stressed polishing on off-axis aspheric lightweight mirrors consisting of SiC or other materials.

© 2020 Optical Society of America under the terms of the OSA Open Access Publishing Agreement

## 1. Introduction

The primary mirror of a large-aperture optical astronomical telescope comprises between a dozen and a thousand off-axis aspheric sub-mirrors, resulting in many high-precision optical mirror processing cycles that hinder the telescope development cycle. Off-axis stressed polishing of an aspheric mirror involves splicing sub-mirrors to use large-diameter tools to grind off-axis aspheric surfaces [1,2]. Aspheric surface processing can be converted to spherical surface processing; hence, large-diameter tools can be used for full-diameter polishing. This greatly improves the processing efficiency and reduces the surface high-frequency error compared with conventional sub-aperture polishing under numerical control [3,4]. At present, this method is used to polish the thin glass plate of the primary mirror of a large ground-based telescope system [5,6].

In modern space science, lightweight manufacturing of mirrors carrying optical remote sensing loads has reduced the weight of the mirror body and the cost of satellite launches. The development of finite element analysis software has led to the integrated optimization design of ultra-lightweight mirrors and made it easier to achieve a lightweight rate of more than 70%. Silicon carbide (SiC) is an ideal material for ultra-lightweight space mirrors owing to its high specific stiffness, low thermal expansion coefficient, good thermal conductivity, and isotropic properties. For example, the Sofia infrared space telescope, jointly developed by NASA and the German Aerospace Agency, has a second mirror that is a 352 mm SiC ultra-lightweight mirror, with a weight of only 1.97 kg and an areal density of 20 kg/m$^2$ [7]. The carbon fiber-reinforced SiC mirror developed by the German Industrieanlagen-Betriebsgesellschaft (IABG) has a diameter

#410759 https://doi.org/10.1364/OE.410759
Journal © 2020 Received 23 Sep 2020; revised 5 Nov 2020; accepted 5 Nov 2020; published 16 Nov 2020

Optics EXPRESS

of 500 mm and an area density of only 8 kg/m$^2$ [8]. These ultra-lightweight SiC mirrors are processed using computer-controlled optical surfacing sub-aperture polishing.

SiC is a brittle material with ceramic characteristics and thus its Mohs hardness is high, the removal rate is low, and the surface shape convergence is slow. Sub-aperture addition methods, such as magnetorheological finishing (MRF) [3,4] and small-tool manufacturing [9], are mainly used to polish off-axis aspheric SiC. The mirror surface is quantized to an RMS precision of 200–300 nm and an ion beam modification is performed. The inherent mid-frequency oscillation of sub-aperture processing inevitably causes mid- and high-frequency errors. Furthermore, the removal volume is small and the processing time is long, which is not compatible with the rapid manufacturing requirements of large-aperture aspheric mirrors. Full-aperture polishing of lightweight mirrors can be achieved if the stressed polishing technology used to process thin glass plate mirrors can be successfully used to process off-axis aspheric SiC lightweight mirrors. However, the physical basis of stressed mirror polishing (SMP) is the theory of small-deflection deformation of a thin elastic plate. The back of the lightweight mirror is a grid-reinforced rib structure and the analytical formula used for a thin-plate mirror cannot be directly used to solve the applied stress distribution.

Thus, we study the feasibility of using SMP to process off-axis aspheric SiC lightweight mirrors. The specific method includes three steps. The first step is to examine the deformability of the lightweight mirror through stressed loading. The second is to establish an optimized model, use a program to search for a thin plate of equivalent thickness, and analyze its deformation. The third is to test different structural models, generalize the equal-thickness thin-plate method, and simulate and polish the optimized model to compare and analyze the surface shape results. To solve the problems of high Mohs hardness, low removal rate, and slow surface convergence of SiC materials, we propose an off-axis aspheric SiC lightweight mirror to minimize removal and improve polishing efficiency. We propose and explain the "iterative initial aspheric method" for SMP. This research aims to provide a new approach for full-aperture polishing of off-axis aspheric SiC lightweight mirrors.

## 2. Physical foundation of SMP technology

Until now, stressed mirror polishing technology has been used in the full-aperture polishing of off-axis aspheric low-expansion glass thin-plate mirrors. Recently, we systematically studied the feasibility of full-aperture polishing of an off-axis aspheric SiC thin plate mirror using stressed polishing technology [10]. Then, whether the SMP technology be transplanted to the off-axis aspheric lightweight mirror full aperture polishing becomes a new problem what we faced. The difficulty is there exist ribs structure on the back of the lightweight mirror, which makes the expression based on the small deflection deformation theory of the elastic thin plate unable to be used to guide the full-aperture stressed polishing of the off-axis aspheric lightweight mirror.

It is difficult to establish corresponding theoretical models owing to the various forms of lightweight mirrors. The simplest method is to adapt the lightweight structure to the theory of small deflection and deformation of elastic thin plates. To form a system with Ref. [10], SiC is still used as a mirror blank material. In addition, without considering the complicated situation of the actual project, such as the hexagonal cutting and installation of the mirror body, the feasibility of the full-aperture stressed polishing of the single off-axis aspheric lightweight mirror is studied from the level of basic methods. If the basic method is feasible, further consideration of the processing of off-axis aspheric light-weight splicing sub-mirrors will have a theoretical and methodological basis.

Subsequently, work was conducted under the coordinate [10,11] system of the large-aperture astronomical telescope and its spliced sub-mirror. Figure 1 shows the distribution of the splicing segments of the primary mirror for a large-aperture telescope.

Optics EXPRESS

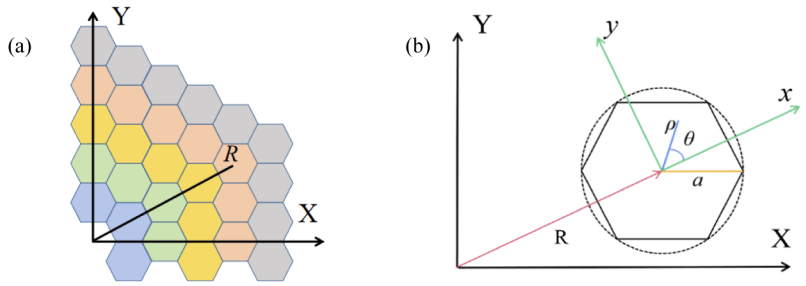


**Fig. 1.** Distribution of splicing segments of the primary mirror of a large-aperture telescope: (a) splicing segment system; (b) local coordinate system on a single segment.

Assume that the radius of the off-axis aspheric mirror is $a$ and that the surface shape of a specific segment mirror can be expressed using the local coordinate system, as shown in Fig. 1(b). The expression for the surface shape is [1]:

$$Z(\rho,\theta)=\sum_{mn}\alpha_{mn}^{seg}\rho^{m}\cos(n\theta). \tag{1}$$

where $m$ and $n$ are integers, $m\geq n\geq 0$ and $m-n$ is an even number. Further, $\rho=(x^2+y^2)^{1/2}/a$, $\theta=\tan^{-1}(y/x)$, and $\alpha_{mn}$ are functional expressions for the mirror geometric parameters that are related to the off-axis quantity, aperture, cone coefficient, and radius of curvature of the mirror, respectively. The explicit equations for $\alpha seg\ mn$ are expressed as follows [1]:

$$\begin{cases}
\alpha_{20}^{seg}=\frac{a^2}{k}\left[\frac{2-K\varepsilon^2}{4(1-K\varepsilon^2)^{3/2}}\right]\\
\alpha_{22}^{seg}=\frac{a^2}{k}\left[\frac{K\varepsilon^2}{4(1-K\varepsilon^2)^{3/2}}\right]\\
\alpha_{31}^{seg}=\frac{a^3}{k^2}\left[\frac{K\varepsilon[1-(K+1)\varepsilon^2]^{1/2}(4-K\varepsilon^2)}{8(1-K\varepsilon^2)^3}\right]\\
\alpha_{33}^{seg}=\frac{a^3}{k^2}\left[\frac{K^2\varepsilon^3[1-(K+1)\varepsilon^2]^{1/2}}{8(1-K\varepsilon^2)^3}\right]\\
\alpha_{40}^{seg}=\frac{a^4}{k^3}\left[\frac{8(1+K)-24K\varepsilon^2+3K^2\varepsilon^4(1-3K)-K^3\varepsilon^6(2-K)}{64(1-K\varepsilon^2)^{9/2}}\right]\\
\alpha_{42}^{seg}=\frac{a^4}{k^3}\left[\frac{K\varepsilon^2[2(1+3K)-(9-7K)K\varepsilon^2+(2+K)K^2\varepsilon^4]}{16(1-K\varepsilon^2)^{9/2}}\right]\\
\alpha_{44}^{seg}=\frac{a^4}{k^3}\left[\frac{K^2\varepsilon^4[1+5K-K\varepsilon^2(6+5K)]}{64(1-K\varepsilon^2)^{9/2}}\right]
\end{cases} \tag{2}$$

where $\varepsilon=R/k$, $R$ is the off-axis quantity, $k$ is the radius of curvature of the surface of rotation, and $K$ is the quadric surface coefficient. Moreover, $\alpha^{seg}$ represents the shape coefficient of the off-axis aspheric mirror of the target surface and $\alpha^{str}$ represents the coefficient produced by the

Optics EXPRESS

application of pre-stress. The corresponding relations are listed as follows [1]:

$$\begin{cases} \alpha_{20}^{str} = a/(2k_B) - \alpha_{20}^{seg}\ (power) \\ \alpha_{22}^{str} = -\alpha_{22}^{seg}\ (astigmatism) \\ \alpha_{31}^{str} = -\alpha_{31}^{seg}\ (coma) \\ \alpha_{33}^{str} = -\alpha_{33}^{seg}\ (trefoil) \\ \alpha_{40}^{\mathrm{str}} = a^4/(8{k_B}^3) - \alpha_{40}^{seg}\ (spherical\ aberration) \\ \alpha_{42}^{str} = -\alpha_{42}^{seg}\ (secondary\ astigmatism) \\ \alpha_{44}^{str} = -\alpha_{44}^{seg}\ (quadrafoil) \end{cases} . \tag{3}$$

here, $k_B$ is the radius of curvature of the segment.

The number of levers stressed by the facility is $N$ and the loading point is in the mirror direction $\theta_{\mathrm{n}}$, where $\theta_{\mathrm{n}} = 2\pi\ (n-1)/N$. The point force and moment are then expressed using the following [12]:

$$\begin{cases} V(\theta_x) = V_1\cos(\theta_n) + V_2\cos(2\theta_n) \\ M(\theta_n) = M_0 + M_1\cos(\theta_n) + M_2\cos(2\theta_n) \end{cases} . \tag{4}$$

where $M$ and $V$ are determined by the surface shape, $E$ is the elastic modulus of the material, $\nu$ is Poisson's ratio of the material, $D$ is the stiffness of the plate, and $h$ is the thickness of the mirror. These parameters are given by the following [12]:

$$\begin{cases} D = \frac{Eh^3}{12(1-\nu^2)} \\ M_0 = (D/a^2)[2(1+\nu)\alpha_{20}^{\mathrm{str}}] \\ M_1 = (D/a^2)[2(3+\nu)\alpha_{31}^{\mathrm{str}}] \\ M_2 = (D/a^2)[2(1-\nu)\alpha_{22}^{\mathrm{str}}] \\ V_0 = 0 \\ V_1 = -\frac{M_1}{a} \\ V_2 = \frac{2M_2}{a} \end{cases} . \tag{5}$$

The approximate radius of the virtual data disk can be written as [1,10]:

$$l = l_0\left(1 + \frac{a^2}{4l_0^2}\right). \tag{6}$$

where $l_0$=$2k/(c+c^3)$, c = cos$\varphi$, and the slope of the $x$-$y$ plane with respect to the $X$-$Y$ plane is $\varphi$=tan$^{-1}\varepsilon$. The optical system parameters used in this study were derived from a scaling model of an optical system. The aspheric surface coefficient was $K = -1$, the radius of curvature of the vertex was 2032mm, the off-axis was 280 mm, and the scaling factor of the optical path reduction was 4.2587. These parameters allow greater deformation of the mirror body than are allowed by the SMP parameters of the splicing sub-mirrors of the existing large-aperture telescopes and those under construction [13]; this is because the stressed polishing needs to be suitable not only for processing off-axis aspheric SiC lightweight single mirrors but also for lightweight spliced sub-mirrors of the main mirror of an astronomical telescope. The simulation method and SMP process can be found in Ref. [10].

Optics EXPRESS

## 3. Equivalent-plate model

The materials that can be used in SMP require uniformity, linearity, complete elasticity, isotropy, and rigidity [1,2]. In practice, the deviation of an optical aspheric surface from a spherical surface is relatively limited and characterized by small deflection deformation. Then, we can use the small-deflection deformation theory for a thin plate to analyze and solve the problem. Although the lightweight structure of the SiC mirror has a back-rib structure, it is still possible to meet the above conditions under certain circumstances. The unknown thin-plate with the same mechanical response as the lightweight mirror may be called the equivalent thin-plate model and the process of finding this model the equivalent thin-plate method. Exploring this problem can help verify the feasibility of stressed polishing of lightweight mirrors.

It is necessary to explore the applicability of stressed polishing to lightweight mirrors before conducting experimental research. The physical basis of SMP is the small-deflection deformation theory of an elastic thin plate, which is used for polishing a thin-plate mirror. To apply this method to the stressed polishing of lightweight mirrors, the thickness and structure of the mirror body must first be determined. This is the motivation for establishing an equivalent thin-plate model.

The basic idea of the equivalent thin-plate method is to apply the same force (unit load) to the lightweight model and a thin-plate model of the same caliber using finite element software. When the displacements of the two actuator ends are the same, we find the thickness of the thin-plate model with the smallest displacement error at the free end of the two. At this time, the force and moment loaded on the lightweight model are the same as those on the equivalent thin-plate model. Figure 2 shows the stress polishing process for the equivalent thin-plate model of the lightweight mirror.

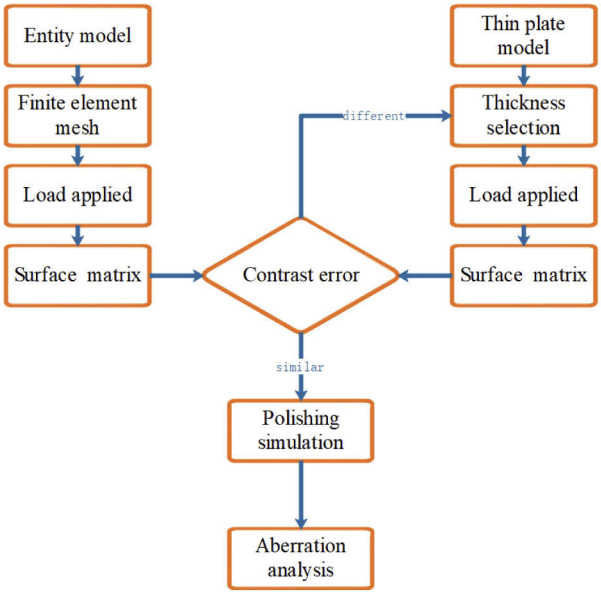


**Fig. 2.** SMP process of an equivalent-thin plate of the lightweight mirror.

According to the process on the left side of Fig. 2, we first establish a solid model of the required lightweight model and limit its area density to within a certain range. This is to ensure that the model can achieve the expected deformation, without affecting the overall strength. Then,

Optics EXPRESS

we perform finite element solid meshing on the model, apply constraints to the freedom of the mirror center, and apply unit loads to the edges to obtain the surface response matrix.

According to the process on the right side of Fig. 2, we first establish a thin-plate model to be determined and take the middle surface of the structure to establish a finite element model. The degree of freedom of the mirror center is also constrained, a unit load is applied to the edge, and the surface response matrix is obtained by adjusting the thickness of the middle surface. We compare the corresponding data of the two sets of response matrices of the lightweight and thin-plate models. The point of maximum mirror deformation is the symmetrical point on the diameter of the loading point about the center of the circle. The loading point is defined as the actuating end and the maximum difference is the free end. The required equivalent thickness needs to be as small as possible for the free-end error. At this time, the thickness is the equivalent thin-plate thickness of the target lightweight mirror.

When the equivalent thickness is obtained, we use the expressions for SMP, i.e., Eqs. (1)–(5), to write a Matlab program with thickness as a variable to obtain the force and moment corresponding to the equivalent thickness of the thin plate. The force and moment are applied to the lightweight mirror body and the equivalent thickness thin-plate mirror body; its deformed surface shape is then substituted into the removal program to obtain the partial aberration and iterative surface shape residual of the two mirror bodies after polishing.

In the removal algorithm, the model takes the surface center point as the zero displacement point during the deformation and polishing removal stages. Under the constraint of the model center point, the center stress value is selected to be less than $10^{-2}$ N [1,10] to complete the stress loading and model change of the off-axis aspheric SiC lightweight mirror. This method places the mirror body in the state of applied loading and the center position of the mirror surface is not removed owing to deformation during polishing to ensure the rationality of the algorithm and simulation.

### *3.1. Concave flat triangular lightweight mirror body*

#### 3.1.1. Finding the equivalent-plate thickness

The model is a triangular lightweight structure that is concave flat, i.e., the reflective surface is concave and the bottom surface is flat. The caliber is 350 mm, the mirror panel thickness is 3 mm, the stiffener thickness is 3 mm, the mirror center height is 10.0 mm, and the edge height is 17.5 mm. The structure of the mirror body is shown in Fig. 3.

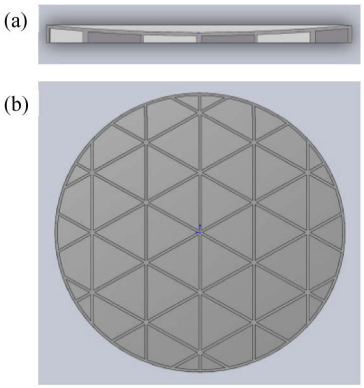


**Fig. 3.** Concave flat lightweight mirror body structure: (a) sectional view; (b) back.

Referring to the literature on a deformable actuated hybrid mirror (AHM) [14], when establishing a lightweight mirror model suitable for bending moment loading, its area density

Optics EXPRESS

should be as low as possible to ensure its deformability. The finite element simulation is enabled by making the calculation converge quickly to the preset target and the surface density of the lightweight mirror is selected in the range of 10–15 kg/m$^2$ to establish the model.

The model is divided into finite elements through the HYPERMESH software and imported to apply a force of 1 unit to the loading point. The change in the mirror surface was investigated. The position of the loading point is selected at the actuating end; the other end is the free end. The actuation deformation is shown in Fig. 4.

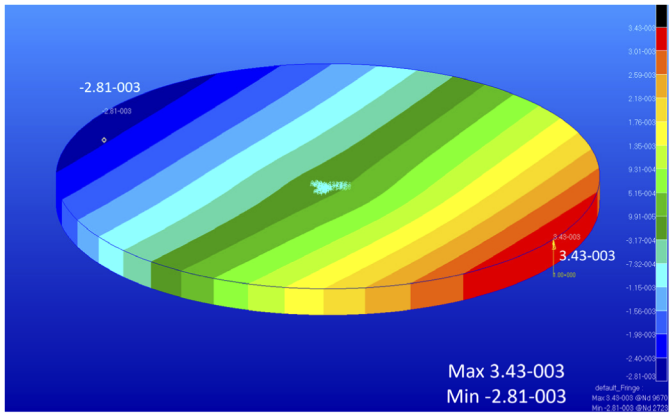


**Fig. 4.** Surface shape of mirror under a unit load.

In Fig. 4, the displacement of the actuation end is 3.43 μm and that of the free end is 2.81 μm. Using these displacements as a reference standard, a comparative SiC thin-plate model is formulated whose caliber and radius of curvature are the same as those of the lightweight model. The initial thickness of the thin plate was 3 mm and the same unit load was applied at the edge loading point. The actual thickness of the thin-plate model can be obtained by coupling the software programs Matlab and Patran. We use thickness as the variable to search for the equivalent model with the same displacement at the actuating end. Figure 5 shows the surface shape of the thin-plate model. The displacement of the actuating end is 3.43 μm and that of the free end is 2.30 μm.

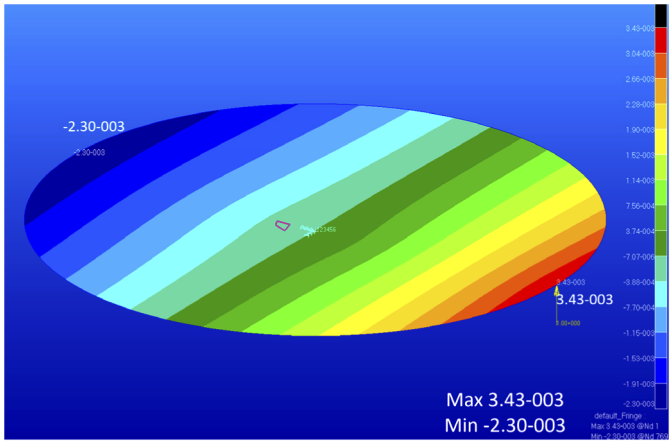


**Fig. 5.** Actuation response of equivalent-plate surface.

Optics EXPRESS

In the model shown in Fig. 5, the surface density of the mirror is 14.6 kg/m$^2$. The thickness of the thin plate is 5.41 mm, which is the same as the displacement of the actuating end of the lightweight model. The free-end error was 22.6%. The following uses a thin plate with this thickness as a model to simulate and analyze the SMP.

### 3.1.2. Simulation of SMP of equivalent thin-plate model

We write a MATLAB program using Eqs. (1)–(5) with the equivalent thickness as a variable to obtain the loading force and moment of the concave flat triangular lightweight mirror under 12-point loading. As presented in Table 1, 12 points are evenly distributed on the edge of the mirror body.

**Table 1. Loading force and moment of concave flat triangular lightweight structure**

| Node | V($x$,$y$,$z$)/N | M($x$,$y$,$z$)/(N·mm) |
|---|---|---|
| 1 | (0,0, −58.57) | (4479.56, −7758.83,0) |
| 2 | (0,0, −61.45) | (4103.19, −2368.98,0) |
| 3 | (0,0, −50.21) | (229.61, 0,0) |
| 4 | (0,0, −20.17) | (−2382.73, −1375.67,0) |
| 5 | (0,0, 14.58) | (−1957.87, −3391.13,0) |
| 6 | (0,0, 30.14) | (0, −4118.95,0) |
| 7 | (0,0, 14.58) | (1957.87, −3391.13,0) |
| 8 | (0,0, −20.17) | (2382.73, −1375.67,0) |
| 9 | (0,0, −50.21) | (−229.61,0,0) |
| 10 | (0,0, −61.45) | (−4103.19, −2368.98,0) |
| 11 | (0,0, −58.57) | (−4479.56, −7758.83,0) |
| 12 | (0,0, −55.29) | (0, −10691.67,0) |

The finite element deformation of the mirror body is obtained through finite element loading, as shown in Fig. 6. We extract the reflective surface node for the subsequent polishing simulation.

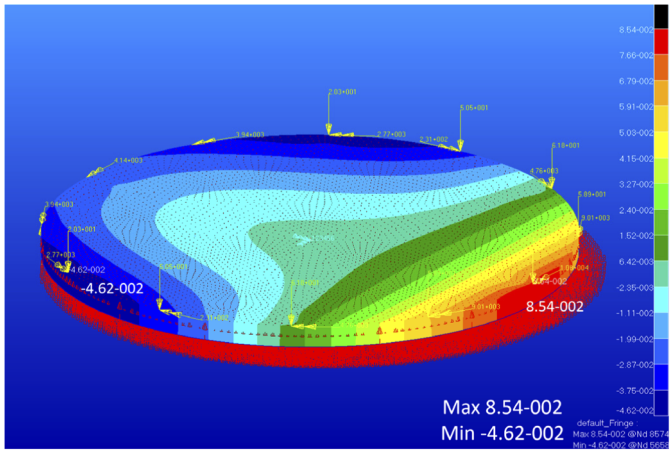


**Fig. 6.** Cloud diagram of the variation of finite element loading of the mirror body.

Optics EXPRESS

We simulated and calculated the inner surface of the 300 mm effective aperture, the lightweight mirror shape, and the equivalent thickness of the thin-plate surface under the same load. Figure 7 shows the three aberrations that controlling the low-order surface shape.

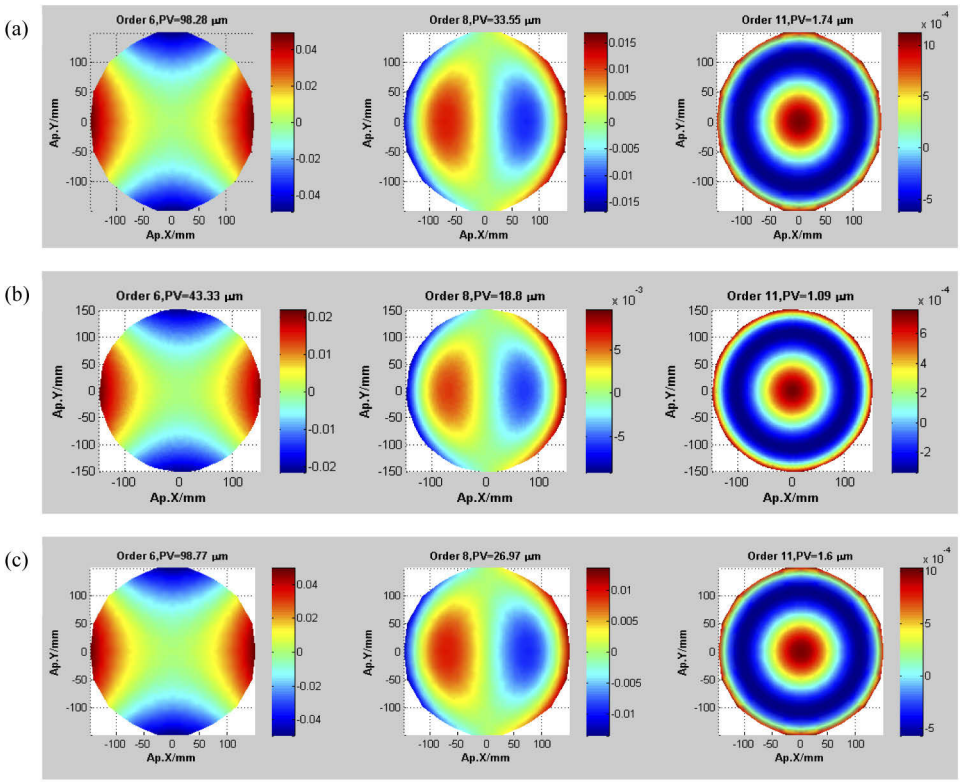


**Fig. 7.** Comparison of surface shape results: (a) theoretically calculated astigmatism, coma, and spherical aberration; (b) astigmatism, coma, and spherical aberration of the parallel triangular lightweight mirror; (c) equivalent-thickness (5.41 mm) astigmatism, coma, and spherical aberration of the thin plate.

In the results in Fig. 7, (a) is the theoretical value of the target surface astigmatism, coma, and spherical aberration; (b) is the simulated lightweight model astigmatism, coma, and spherical aberration; and (c) is the simulated thin-plate model astigmatism, coma, and spherical aberration. The results of (b) and (c) are significantly different, indicating that the 5.41 mm model is not a thin-plate mirror of equivalent thickness for the lightweight mirror body.

### *3.2. Parallel concave triangular lightweight mirror body*

#### 3.2.1. Finding the equivalent-plate thickness

To find a lightweight structure with an equivalent thin-plate model, we adopt a structural solution with the back parallel to the mirror surface. A mirror, structured as shown in Fig. 8, was designed within the areal density requirements. The overall thickness of the mirror body was 10 mm, the panel thickness was 3 mm, the lightweight structure was 7 mm high, and the areal density was 12.46 kg/m$^2$.

As in 3.1.1, the lightweight model has a displacement of 3.88 μm at the actuating end and a displacement of 2.67 μm at the free end, as shown in Fig. 9(a), and the equivalent thickness of the thin plate is 5.17 mm.

Optics EXPRESS

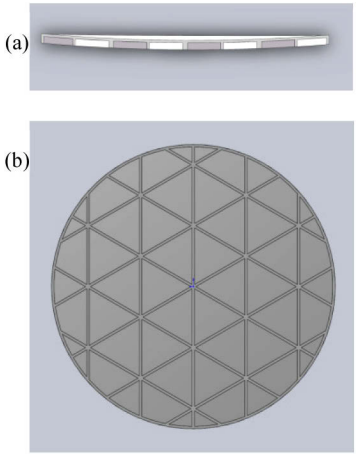


**Fig. 8.** Parallel concave triangular lightweight mirror structure: (a) cross-sectional view; (b) back structure.

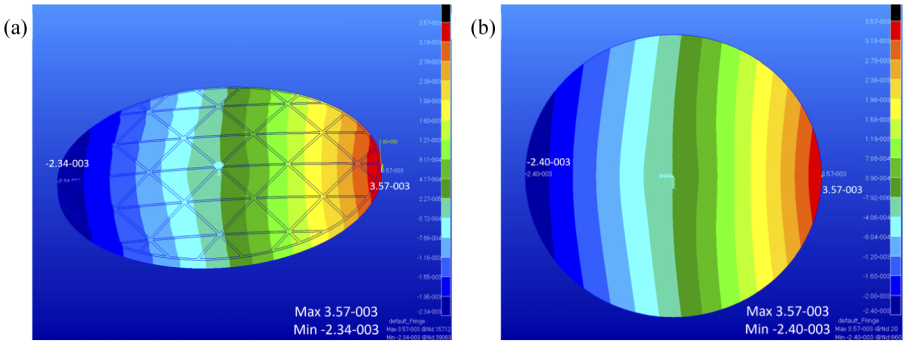


**Fig. 9.** Cloud diagram of the mirror body under a unit load: (a) parallel triangular lightweight mirror body; (b) equivalent thin-plate model.

As shown in Fig. 9(b), the displacement of the actuating end is 3.88 μm and that of the free end is 2.60 μm under the unit load of the equivalent thin plate. The free-end error between the lightweight model and equivalent thin-plate model was only 2.6%. In this model, the equivalent thin plate and lightweight mirror have good response consistency under the same unit load. This consistency is also reflected in the sub-aberration comparison.

### 3.2.2. Simulation of SMP of the equivalent thin-plate model

As in 3.1.2, we obtain the load force and moment data of the parallel concave triangular lightweight mirror body in the 12-point mode, as shown in Table 2.

We simulated and calculated the inner surface of the 300 mm effective aperture, the lightweight mirror shape, and the surface shape of the thin plate with equivalent thickness. Figure 10 shows the aberration results for the low-order surface shape.

Figure 10 shows that there is no significant difference between the results of (b) and (c), indicating that the thin-plate model with a thickness of 5.17 mm is the equivalent of the lightweight mirror body.

Optics EXPRESS

**Table 2. Loading force and moment of parallel concave triangular lightweight structure**

| Node | V(*x*,*y*,*z*)/N | M(*x*,*y*,*z*))/(N·mm) |
|---|---|---|
| 1 | (0,0, −51.40) | (3931.18, −6809.00,0) |
| 2 | (0,0,−53.93) | (3600.86, −2078.96,0) |
| 3 | (0,0, −44.06) | (201.44, 0,0) |
| 4 | (0,0, −17.70) | (−2091.10, −1207.30,0) |
| 5 | (0,0, 12.80) | (−1718.23, −2976.06,0) |
| 6 | (0,0, 26.45) | (0, −3614.79,0) |
| 7 | (0,0, 12.80) | (1718.23, −2976.06,0) |
| 8 | (0,0,−17.70) | (2091.10, −1207.30,0) |
| 9 | (0,0,−44.06) | (−201.44,0,0) |
| 10 | (0,0, −53.93) | (−3600.86,– 2078.96,0) |
| 11 | (0,0, −51.40) | (−3931.18,– 6809.00,0) |
| 12 | (0,0, −48.52) | (0, −9382.82,0) |

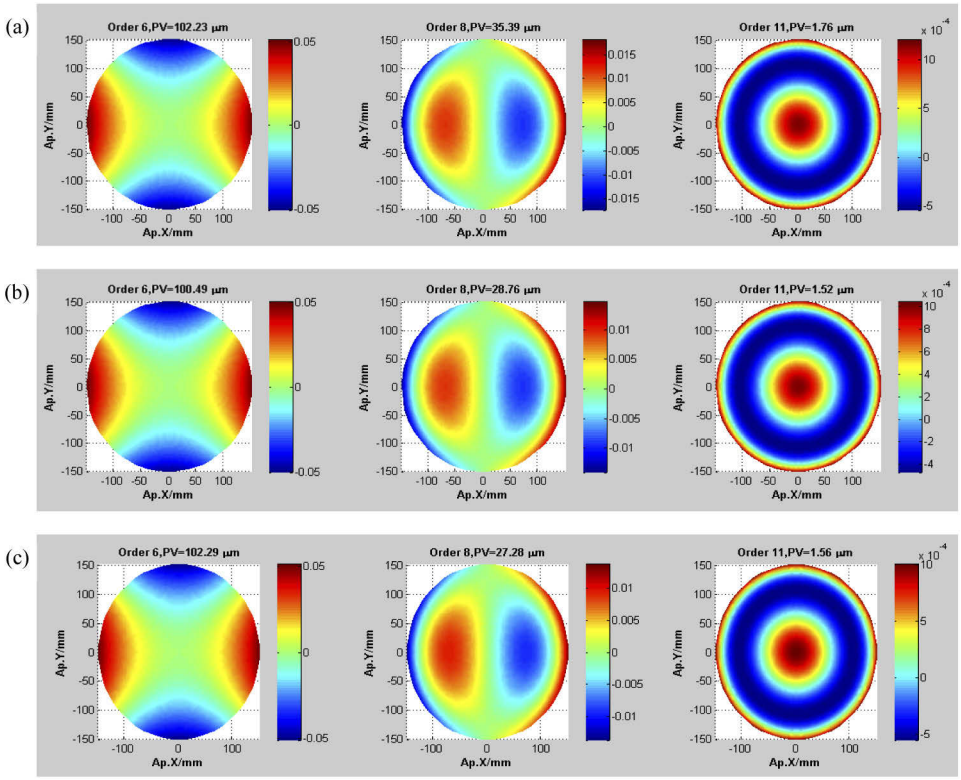


**Fig. 10.** Comparison of surface shape results: (a) theoretically calculated astigmatism, coma, and spherical aberration; (b) astigmatism, coma, and spherical aberration of the parallel triangular lightweight mirror; (c) equivalent-thickness (5.17 mm) astigmatism, coma, and spherical aberration of the thin plate.

Optics EXPRESS

### 3.3. Parallel concave fan-shaped lightweight mirror blank

#### 3.3.1. Finding the equivalent-plate thickness

To determine whether this method is suitable for other back structures, we selected a lightweight model of a fan-shaped back structure with 12-point loading. The panel thickness of the lightweight mirror was 3 mm, the overall thickness was 10 mm, and the surface density was 11.95 kg/m$^2$. Figure 11 shows the fan-shaped back structure of the lightweight mirror.

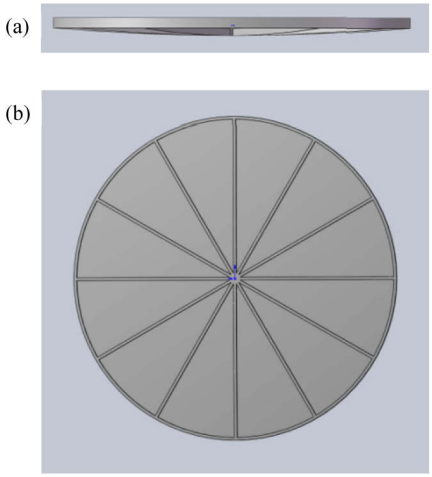


**Fig. 11.** Parallel concave fan-shaped lightweight mirror structure: (a) sectional view; (b) back structure.

As in 3.1.1, the displacement of the actuation end of the lightweight model is 4.74 μm, and the displacement of the free end is 2.84 μm, as shown in Fig. 12(a). The equivalent thickness of the thin plate is 4.81 mm.

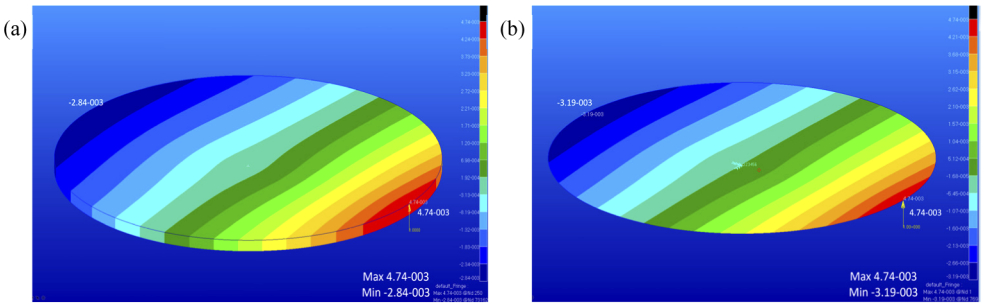


**Fig. 12.** Cloud diagram of the mirror body under unit load: (a) parallel fan-shaped lightweight mirror body; (b) equivalent thin-plate model.

As shown in Fig. 12(b), the displacement of the actuating end is 4.74 μm and that of the free end is 3.19 μm under the unit load of the equivalent thin plate. The free-end error between the lightweight and equivalent thin-plate model was 12.3%.

#### 3.3.2. Simulation of SMP of the equivalent thin-plate model

As in 3.1.2, we obtain the data of the loading force and moment of the parallel concave fan-shaped lightweight mirror body under 12-point loading, as presented in Table 3.

Optics EXPRESS

**Table 3. Loading force and moment of parallel concave fan-shaped lightweight structure**

| Node | V($x$,$y$,$z$)/N | M($x$,$y$,$z$)/(N·mm) |
|---|---|---|
| 1 | (0,0, −41.39) | (3165.79, −5483.31,0) |
| 2 | (0,0, −43.43) | (2899.76, −1674.17,0) |
| 3 | (0,0, −35.48) | (162.16, 0,0) |
| 4 | (0,0, −14.26) | (−1684.04, −972.28,0) |
| 5 | (0,0, 10.30) | (−1383.74, −2396.71,0) |
| 6 | (0,0, 21.30 | (0, −2911.09,0) |
| 7 | (0,0, 10.30) | (1383.74, −2396.71,0) |
| 8 | (0,0, −14.26) | (1684.04, −972.28,0) |
| 9 | (0,0, −35.48) | (−162.16,0,0) |
| 10 | (0,0, −43.43) | (−2899.76, −1674.17,0) |
| 11 | (0,0, −41.39) | (−3165.79, −5483.31,0) |
| 12 | (0,0, −39.07) | (0, −7556.03,0) |

We simulated and calculated the inner surface shape of the 300 mm effective aperture, the lightweight mirror shape, and the equivalent thickness of the thin-plate surface. Figure 13 shows the aberration results of the low-order surface shape.

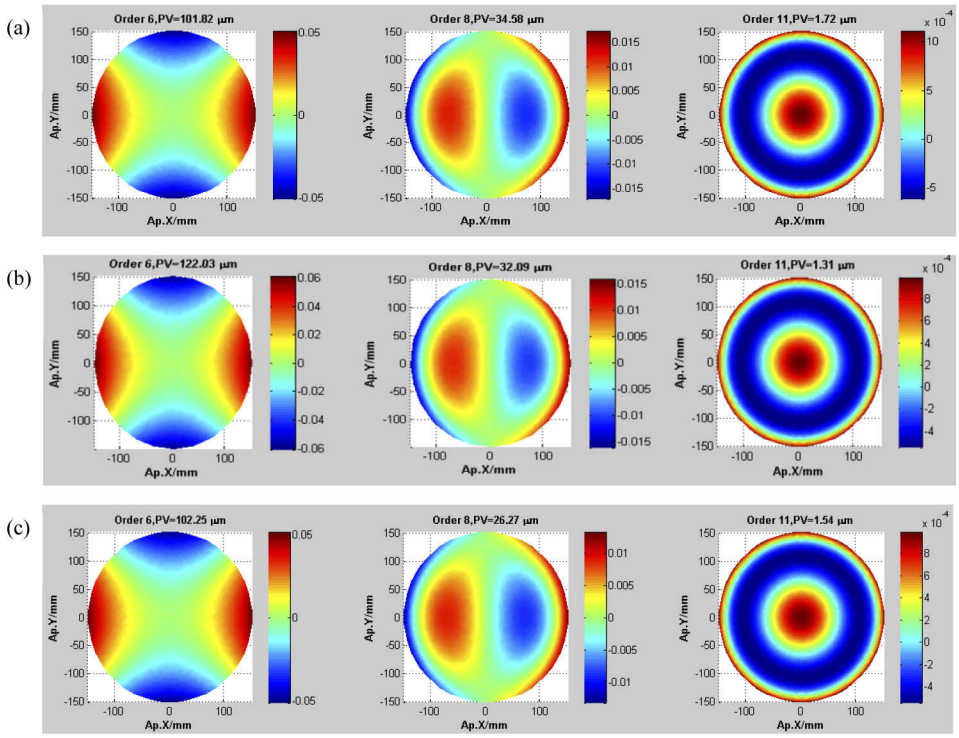


**Fig. 13.** Comparison of surface shape results: (a) theoretically calculated astigmatism, coma, and spherical aberration; (b) astigmatism, coma, and spherical aberration of the parallel fan-shaped lightweight mirror; (c) equivalent-thickness (4.81 mm) astigmatism, coma, and spherical aberration of the thin plate.

Optics EXPRESS

Figure 13 shows that the astigmatism and coma in the results of (b) and (c) are significantly different, indicating that the thin-plate model with a thickness of 4.81 mm is not the equivalent of the lightweight mirror body.

### 3.4. Results and discussion

#### 3.4.1. Mechanical responses of the three models

Table 4 sorts the simulation results for the above lightweight mirror obtained via the equivalent thickness thin-plate method. The calculation method of the error percentage is as follows: The free end displacement of the lightweight mirror and the equivalent thin-plate mirror is subtracted, and calculate the proportion of the difference with the displacement of the free end of the equivalent thin plate mirror to obtain the error percentage.

**Table 4. Mechanical response data of the three models**

| Mirror blank structure | Mirror form | Actuating end | Free end | Error percentage |
|---|---|---|---|---|
| Concave flat structure | Triangle lightweight | 3.43μm | 2.81μm | 22.1% |
| | Equivalent thin-plate | 3.43μm | 2.30μm | |
| Parallel concave structure | Triangle lightweight | 3.88μm | 2.67μm | 2.6% |
| | Equivalent thin-plate | 3.88μm | 2.60μm | |
| Parallel concave structure | Fan-shaped lightweight | 4.74μm | 2.84μm | 12.3% |
| | Equivalent thin-plate | 4.74μm | 3.19μm | |

Table 4 demonstrates that among the three structural models, only the lightweight mirror with the parallel concave triangular structure and its equivalent-thickness model match the actuation response of the unit load to a high degree; the error is only 2.6%. The actuation response error of the free ends to the unit load is too large for the other two models, which would cause the aberration of the mirror polished under the load force, determined via the equivalent thickness, to be inconsistent with the theoretical value, as shown in Figs. 7 and 13. Moreover, Table 4 demonstrates that when the surface density of the mirror body increases outwardly from the center of the mirror surface, the value at the free end of the lightweight mirror body is greater than that at the free end of the equivalent thin plate. When the trend is small, the free-end value of the lightweight mirror body is lower than that of the equivalent thin plate. The aberration PV value of the lightweight model has a large deviation from that of the thin-plate model; i.e., there is no corresponding equivalent thin-plate model.

#### 3.4.2. Basic law of structure selection

The simulation demonstrates that the existence of an equivalent thin-plate model for a lightweight mirror body depends on whether the body has uniform areal density and isotropic bending properties. In Models 1 and 3 of this article, the concave flat triangular lightweight mirror body gradually increases in density from the inside to the outside and the density of the parallel concave fan-shaped lightweight mirror body gradually decreases from the inside to the outside. This causes the lightweight mechanical response of the free end to be different from that of the free end of the equivalent thin plate. However, the parallel concave triangular lightweight mirror body of Model 2 has both a uniform and low areal density and a corresponding thin plate of equivalent thickness.

#### 3.4.3. New lightweight mirror blank design

From the above, we observe that the design of the off-axis aspheric lightweight mirror that is to be stress-polished and full-aperture processed is different from that of the mirror blank that undergoes CCOS sub-aperture processing. The lightweight mirror needs to be molded from the

Optics EXPRESS

mirror blank according to the final parameters used. Initially, it is necessary to design the outline of the mirror blank, the lightweight topology of the mirror body, and the polishing form. This may be referred to as the stressed-polishing ab initio design of the off-axis aspheric lightweight mirror. When considering the lightweight rate of the mirror body, the focus should be on the design of the mirror body profile, surface density uniformity and isotropic bending properties. For example, Models 1 and 3 have no corresponding equivalent thickness thin-plate mirror because their surface densities are not uniform, so full-aperture stressed polishing is not possible.

However, Table 4 shows that when the displacement of the actuating end of the concave flat triangular lightweight structure (with surface density increasing from the center) is 3.43 μm, the displacement of the free end is lower (2.30 μm). When the displacement of the actuating end of the parallel concave fan-shaped lightweight structure (with surface density decreasing from the center) is 2.84 μm, the displacement of the free end is greater (3.19 μm). We can conclude from this that if the lightweight structure of Model 1 is sparse and dense inside so that the surface density of the mirror blank is uniform, we can find the corresponding thin plate of equivalent thickness. The design process for the fan-shaped lightweight structure of Model 3 is essentially the same: if the contour of the mirror blank is optimized to a concave flat structure so that the surface density of the blank is uniform, then the corresponding equivalent thickness can also be found.

#### 3.4.4. Load stress and moment

The thickness of the thin-plate mirror body obtained from the three-structure lightweight mirror body is different. The differences in the loading stresses and moments of Tables 1–3 are obvious. Therefore, by finding a thin-plate model with the same mechanical response as that of the lightweight mirror body, we can conveniently apply stress polishing based on the theory of small-deflection deformation of an elastic thin plate; i.e., we use Eqs. (1)–(5) to calculate the stress loading and simulate polishing.

#### 3.4.5. Aberration and structure

Figure 10 shows that among the three low-order aberrations of the parallel concave triangular structure with an equivalent thin plate, the astigmatism and spherical aberration closely align while the coma exhibits difference.

For this reason, the stressed loading simulation was performed on thin plates with panel thicknesses of 10 mm and 5 mm. The results are shown in Fig. 14.

Figure 14 shows that when the panel thickness is changed from 10 mm to 5 mm, the coma matches less after processing; this is caused by the increased ratio of the removal thickness to the overall mirror thickness under the same removal thickness, affecting the thin-plate characteristics of the mirror body itself and resulting in errors. The question that needs to be discussed next is how to select a suitable panel thickness range without affecting deformability while ensuring processing capacity.

Changing the surface density also improves the aberrations of the parallel concave triangular and parallel concave fan-shaped lightweight mirrors. When the surface density of the mirror body decreases from the inside to the outside, the coma calculated using the finite element method is closer to the theoretical value but at the cost of compounded astigmatism. Therefore, topology optimization of lightweight structures requires balancing the two factors to achieve better partial aberrations.

#### 3.4.6. Removing the impact on the results

Figure 15 shows the iterative residual results for the parallel concave triangular lightweight mirror body and the equivalent thin plate. The RMS value is approximately the same and there is no significant difference between the lightweight structure and equivalent mirror body. We can

Optics EXPRESS

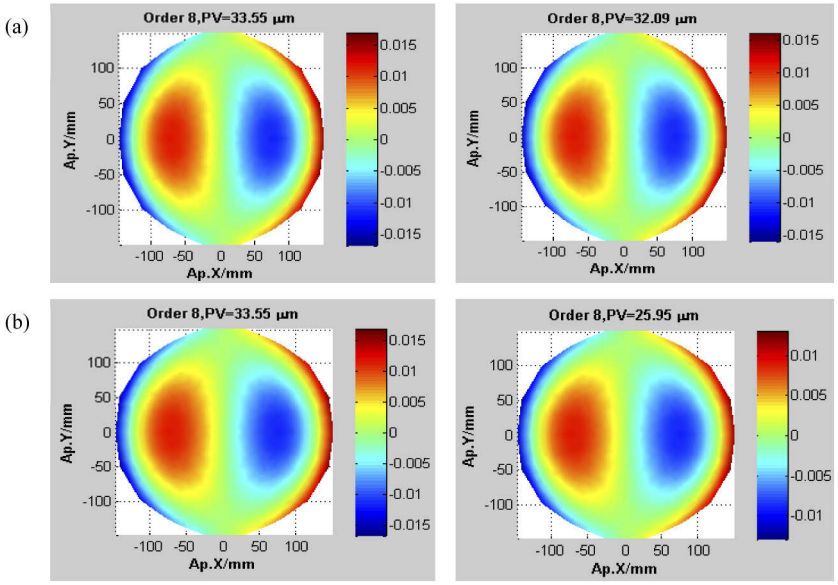


**Fig. 14.** Influence of mirror thickness on coma: (a) theoretical coma and finite element simulation coma of 10 mm mirror body; (b) theoretical coma and finite element simulation coma of 5 mm mirror body.

infer that the method has the same ability to suppress medium- and high-frequency errors in the lightweight mirror body as stress polishing of the thin-plate mirror. Thus, a stable low-order surface shape can be obtained. Although the edge of the lightweight mirror body is affected by the loading position, its local deformation is large, as shown in Fig. 15(b). This has a certain impact on the polishing result but the effect can be eliminated by further controlling the effective aperture. The polishing results meet the range of requirements for subsequent ion beam modification.

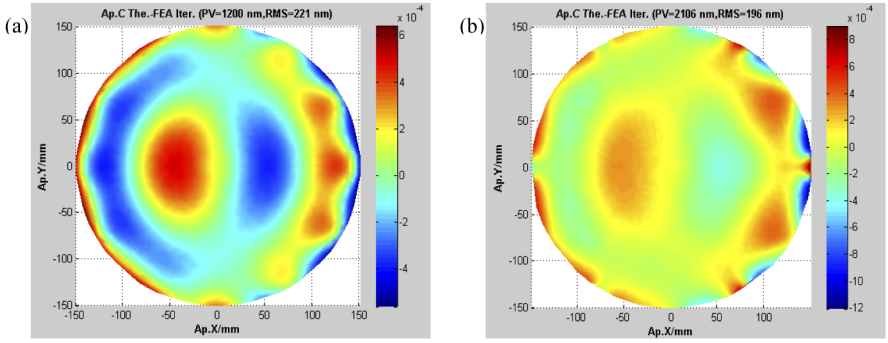


**Fig. 15.** Comparison of surface shape residuals: (a) iterative results for equivalent-plate surface shape residuals; (b) iterative results for lightweight specular shape residuals.

Optics EXPRESS

## 4. Conceptual design of stress-loading equipment and rapid processing methods

### 4.1. Conceptual design of stress-loading equipment

Our laboratory-type stress-loading device adopts an epitaxial loading mechanism, which has a simple structure and is convenient for disassembly and experimentation. It can work with a medium-sized single-axis polishing machine. The loading structure is constructed by combining the Thirty Meter Telescope (TMT) [13], the European Extremely Large Telescope (E-ELT) [15], and Nelson's classic work [1,2] on SMP and adding new simulation methods. The platform structure of the mirror model and the loading rod bonding part are designed in combination with a lightweight simulation mirror. Figure 16 shows the back structure of the mirror body.

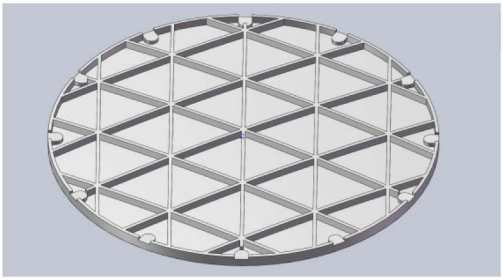

**Fig. 16.** Back structure of the mirror body.

The overall effect is shown in Fig. 17. A layer of rubber padding is added under the mirror body to provide uniform pressure to offset the stress generated in the center of the mirror body from applying a force. The use of rubber pads here is a conceptual design. In practical applications, due to the lightweight structure, the supporting device will be a part that needs to be considered. The more reliable solution here is to use a whiffle-tree structure or an array of hydraulic cushions for support, but unlike thin plate mirrors [10], the arrangement of support points requires special calculations based on the position of the lightweight ribs. In subsequent experiments, we will also conduct a more in-depth study on the support method and support location. Above the stressed loading equipment is a schematic of a full-diameter polishing disc.

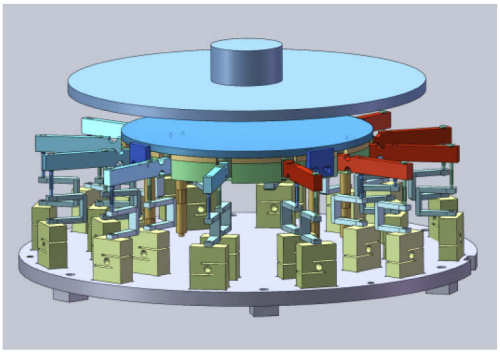

**Fig. 17.** Lightweight stressed polishing equipment.

Optics EXPRESS

### 4.2. Iterative initial aspheric method

The Mohs hardness scale of SiC is greater than 9 (7 for fused silica and 6.5 for crystallites) and thus the time required to remove the material by grinding per unit thickness is approximately five times that of glass; this extremely low removal efficiency is sufficient to offset the advantages of SMP. Hence, we propose an "iterative initial aspheric method" for rapid pre-stressing of off-axis aspheric SiC lightweight mirrors to improve polishing efficiency.

This method consists of four steps:

(1) When the mirror blank of the SiC lightweight mirror is injection-molded, the mirror surface is directly constrained by an abrasive tool to a surface shape that is close to the target off-axis aspheric shape.

(2) The SiC lightweight mirror blank, which has a shape close to that of the target off-axis aspheric surface, is secondarily processed into the initial rough surface shape of the target off-axis aspheric surface.

(3) We applied an external load to transform the mirror blank into a rough approximate surface closest to the spherical surface and polish the spherical surface.

(4) After the load is released, we form a predetermined off-axis aspheric smooth surface that can be modified by subsequent ion beams.

At present, there are many technical means to grind a SiC lightweight mirror blank for processing into a target aspheric surface using a rough surface. It is not difficult to directly make the SiC lightweight mirror into the target shape. The iterative initial aspheric method is feasible.

## 5. Conclusion

We studied the stress polishing and rapid processing of a lightweight SiC mirror to achieve full-aperture polishing of off-axis aspheric splicing sub-mirrors. The physical SMP basis is the theory of small deflection and deformation of an elastic thin plate and it had not previously been applied to a lightweight mirror. This paper proposed an equivalent thin-plate method for the stressed loading of a lightweight mirror. We performed calculations for three types of off-axis aspheric SiC lightweight mirrors under load and demonstrated our method using finite element analysis and the preliminary rules of lightweight structures. The results show that the equivalent thin-plate model can be found by choosing the appropriate lightweight structure and simulating it with a relatively uniform areal density distribution. This unifies the theory for the SMP of lightweight mirrors and thin-plate mirrors. We also proposed an iterative initial aspheric method for stressed polishing of off-axis aspheric SiC lightweight mirrors to improve efficiency and accuracy and designed the corresponding mirror blank manufacturing and polishing steps. This work has shown the feasibility of applying SMP to the rapid production of off-axis aspheric lightweight mirrors.

## Funding

National Key Research and Development Program of China (2016YFB0500100); National Natural Science Foundation of China (11873007, 61975201).

## Disclosures

The authors declare no competing financial interest.

Optics EXPRESS

## References


1. J. Lubliner and J. E. Nelson, "Stressed mirror polishing. 1: a technique for producing nonaxisymmetric mirrors," Appl. Opt. **19**(14), 2332–2340 (1980).
2. J. E. Nelson, G. Gabor, L. K. Hunt, J. Lubliner, and T. S. Mast, "Stressed mirror polishing. 2: fabrication of an off-axis section of a paraboloid," Appl. Opt. **19**(14), 2341–2352 (1980).
3. L. Li, D. Xue, W. Deng, X. Wang, Y. Bai, F. Zhang, and X. Zhang, "Positive dwell time algorithm with minimum equal extra material removal in deterministic optical surfacing technology," Appl. Opt. **56**(32), 9098–9104 (2017).
4. D. Wang, H. Hu, L. Li, Y. Bai, X. Luo, D. Xue, and X. Zhang, "Effects of the gap slope on the distribution of removal rate in Belt-MRF," Opt. Express **25**(22), 26600–26614 (2017).
5. R. Jedamzik, C. Kunisch, and T. Westerhoff, "ZERODUR for stress mirror polishing," Proc. SPIE **8126**, 812606 (2011).
6. R. Jedamzik, C. Kunisch, T. Westerhoff, U. Müller, and J. Daniel, "ZERODUR for stressed mirror polishing II: improved modeling of the material behavior," Proc. SPIE **8450**, 84504P (2012).
7. M. Fruit, P. Antoine, J. Varin, H. Bittner, and M. Erdmann, "Development of the SOFIA silicon carbide secondary mirror," Proc. SPIE **4857**, 274–285 (2003).
8. J. B. Hadaway, R. Eng, H. P. Stahl, J. R. Carpenter, J. R. Kegley, and W. D. Hogue, "Cryogenic performance of lightweight SiC and C/SiC mirrors," Proc. SPIE **5487**, 1018–1029 (2014).
9. H. Hu, X. Zhang, V. Ford, X. Luo, E. Qi, X. Zeng, and X. Zhang, "Edge control in a computer controlled optical surfacing process using a heterocercal tool influence function," Opt. Express **24**(23), 26809–26824 (2016).
10. L. Yi, X. Zhang, H. Hu, Z. Zhang, K. Hai, X. Luo, and D. Xue, "Comprehensive study of the rapid stressed mirror polishing method for off-axis aspheric SiC thin-plate mirrors," Opt. Express **28**(22), 32802–32818 (2020).
11. T. S. Mast, J. E. Nelson, and G. E. Sommargren, "Primary mirror segment fabrication for CELT, " *Proc. SPIE* 4003 (2000).
12. X. Li, Z. Jiang, X. Gong, H. Zhang, K. Chen, Y. Zheng, B. Li, B. Yu, and Q. Xu, "Stressed mirror annular polishing for scale-down TMT primary segments," Proc. SPIE **9912**, 99120A (2016).
13. S. F. Sporer, "TMT: stressed mirror polishing fixture study," Proc. SPIE **6267**, 62672R (2006).
14. L. E. Cohan and D. W. Miller, "Integrated modeling for design of lightweight, active mirrors," Opt. Eng. **50**(6), 063003 (2011).
15. E. Hugot, A. Bernard, M. Laslandes, J. Floriot, T. Dufour, D. Fappani, J. M. Combes, and M. Ferrari, "Stress polishing demonstrator for ELT M1 segments and industrialization," Proc. SPIE **9145**, 914539 (2014).


159.226.165.16 {ts '2021-04-12 02:12:57'}